Strategic integration of battery energy storage and photovoltaic at low voltage level considering multiobjective cost-benefit

Samarjit PATNAIK*⬤**, Manas Ranjan NAYAK**⬤**, Meera VISWAVANDYA**⬤

Department of Electrical Engineering, Biju Patnaik University of Technology, Rourkela, India

Abstract: Renewable energy sources, such as solar photovoltaic (PV) systems and battery energy storage systems (BESS), help reduce greenhouse gas emissions while fulfilling the world's growing energy demand. The inclusion of BESS reduces the peak hour demand, and control of charging and discharging of BESS can be economical for distributors facing time-based energy pricing. This paper discusses a novel multiobjective Horse herd optimisation algorithm (MOHHOA) approach, which is inspired by the social behaviour of horses in herds for PV and BESS optimal allocation in the radial distribution system. The proposed algorithm combines multiple benefits like benefits from economic gain per day, reduction in CO_2 emission per day, and reduction in energy loss per day. IEEE 69-bus radial distribution system (RDS) is used for testing the suggested approach. The case studies and simulation results show that the suggested model effectively accommodated PV power generation in IEEE 69-bus RDS without violating any system constraints. Results indicate improvement in node voltage profiles, security margins and energy losses, and peak energy savings, and system characteristics as a whole, and there were significantly improved techno-economic performance of the distribution system.

Key words: Solar photovoltaic systems, battery energy storage system, multiobjective Horse herd optimisation algorithm (MOHHOA), radial distribution system (RDS) network

1. Introduction

The increasing penetration of photovoltaic solar energy in distribution networks has garnered widespread attention worldwide. Projects that include a battery energy storage system (BESS) gets higher attention due to their practicality, advantages, and commitment to global decarbonisation. According to Wong et al. [1], the addition of BESS to the distribution system improves the voltage profile of the lines, reduces system losses, and increases overall efficiency. BESS, in general, offer both technological and economic benefits. Other relevant requirements such as round-trip efficiency, charging, and discharging power should also be addressed while modelling BESS. These features are distinct and vary according to the BESS characteristics and discharge time requirement as discussed by Pawan et al. [2]. BESS serves a diverse and complex role in the power system network and is expected to continue to do so in the long term. BESS's primary objective is to keep the electric grid within operating limitations and constraints. According to various power system framework partners, BESS is used on the generating and distribution sides and the user end side. In this respect, the articles reviewed are from the generation side, offer stable capacity, minimise investment and operating costs, and consumer perspective: demand response, capacity contract savings, energy arbitrage, and peak shaving as per Alam et al. [3] and Kalantari et al. [4] .

---

*Correspondence: patnaik.samarjit@gmail.com

Numerous types of studies have been conducted on the optimum planning of renewable energy systems (RES) and BESS. Nick et al. [5] is one of the earliest works in this field, focusing on optimum design of PV, BESS, and distributed static compensators to enhance the distribution system's technical, economic, and environmental dependability. Sabori et al. [6] proposed a technique for optimally allocating PV and BESS to maximise economic advantages for a distribution company (DISCO). Talent et al. [7] proposed the distribution system operator's (DSO) viewpoint addresses the optimum size and siting of BESS and distributed generation (DG) to reduce overall investment costs while maximising return through transacted services in the distribution market. BESS and DG locations are chosen to optimise DISCO's profit and ignore the transmission access charge. Salehi et al. [8] presented a novel risk-based approach for determining optimum BESS unit and wind turbine placement and capacity. To reduce yearly distribution network operating costs, Mahdavi et al. [9] proposed a two-level planning method to plan the installation of BESS and DG and establish an hourly optimum operation strategy for BESS and DG. Optimising PV and BESS size to save investment costs while ensuring electricity supply dependability does not consider emissions as per Li et al. [10]. It takes into multi-objective analysis but omits BESS planning and operation optimisation by Mahmood et al. [11]. Several swarm intelligence (SI) algorithms are derived from life rules, hunting, defence systems, gravitational laws, gradient-based techniques discussed by Li et al. [12] and He et al. [13]. Despite the vast number of methods developed, none can address all optimisation issues. The no free lunch (NFL) theorem logically proves this. We proposed a novel SI method to describe the social behaviour of horses in a herd mathematically. Multiobjective Horse herd optimisation algorithm (MOHHOA) has a very good performance in solving complex problems in high dimensions, due to the large number of control parameters based on the behaviour of horses at different ages. The horse herd optimisation algorithm is compared to those of several other optimization algorithms, including the gray wolf optimizer, the sine cosine algorithm, the multiverse optimizer, the dragonfly algorithm, and the grasshopper optimization algorithm using Uni-modal and multi-modal benchmark functions by Naeimi et al [14]. This shows that the proposed algorithm is highly efficient for high dimensional global optimisation problems. The MOHHOA also outperforms the mentioned popular optimisation problems for the case of accuracy, efficiency and complexity. Grid-connected PV-BESS uses a multi-objective evolutionary algorithm to maximise battery capacity and operational parameters as discussed by Mikael et al. [15] and Das et al. [16]. An environmental/economic dual-objective optimisation issue has been addressed in Duchaud et al. [17], and RES and BESS energy optimisation is suggested as the best solution. Using an interdisciplinary approach, Balhtiari et al. [18] and Sawle et al. [19] illustrates a multiobjective optimum design for a hybrid renewable energy system incorporating technological, economic, and social goals. BESS benefits the environment by decreasing CO2 emissions from fossil-fuel-based power plants. Previous work has not addressed how to improve the performance of swarm intelligence algorithms by limiting the search space and effectively optimising multiobjectives. Consequently, this study develops an environmental-based techno-economic multiobjective function using the MOHHOA to condense the search area and enhance the performance of the optimisation method.

The significant contributions of this paper are summarised as follows: (1) In this study, a multi-objective function is defined considering the maximise benefit-cost function, which includes benefits from economic gain per day (energy price arbitrage of a power market, reduction in transmission access charge, operation, maintenance, replacement & investment cost of PV & BESS) , reduction in CO_2 emission per day and reduction in energy loss per day. (2) A novel multiobjective Horse Herd Optimisation algorithm is proposed in this work. The ideal economic, environmental, and technical goals are obtained first, followed by Pareto-

optimal solutions. (3) This article proposes optimum PV and BESS allocation and size in distribution networks considering economic, environmental, and technical goals. (4) The system's performance in terms of voltage profile, security margin, power loss etc. have been analysed after integration of PV and BESS. (5) BESS's charging and discharging profile have been analysed considering the time of use energy pricing.

The following is the structure of this article: Section 2 formulates the mathematical modelling of photovoltaic system, BESS system, radial distribution system and load patterns. Section 3 demonstrates how to describe an objective function and system operational constraints mathematically. Section 4 describes the novel multiobjective horse herd optimisation algorithm (MOHHOA) and comparison with other multiobjective algorithms. Section 5 covers the case study on IEEE 69-bus Radial distribution system (RDS) system and the simulation results and discussion. Finally, Section 6 concludes our research.

2. System modelling

The solar PV and BESS each provide direct current (DC), and the power is transferred through an individual DC/DC converter for PV and BESS, where PV converter is unidirectional and for battery bidirectional converter is used. A bidirectional inverter converts the DC electricity produced by the solar photovoltaic panel and BESS to alternating current. The system's basic configuration is shown in Figure (1).
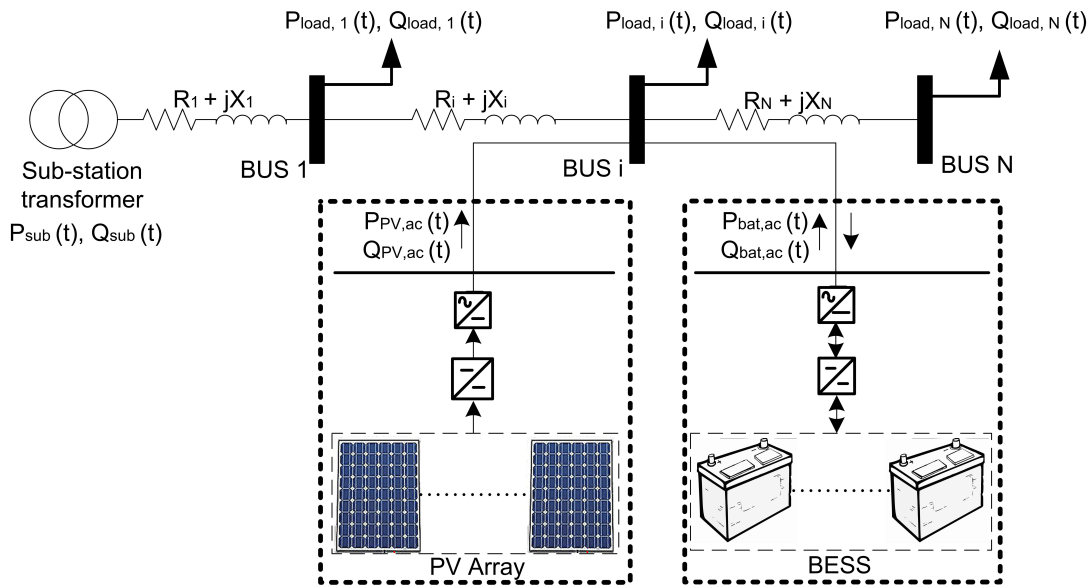
Figure 1. Radial distribution system with PV and BESS.

2.1. Modelling of PV

Solar irradiance has a significant effect on the output power of photovoltaic systems. The solar insolation as per Figure (2) and temperature data as per Figure (3) has been collected for one year (2019) from India Meteorological Department (IMD) Met Centre Bhubaneswar in Bhoi et al. [20]. The Solar output power as a function of solar irradiance is expressed as Equation (1).
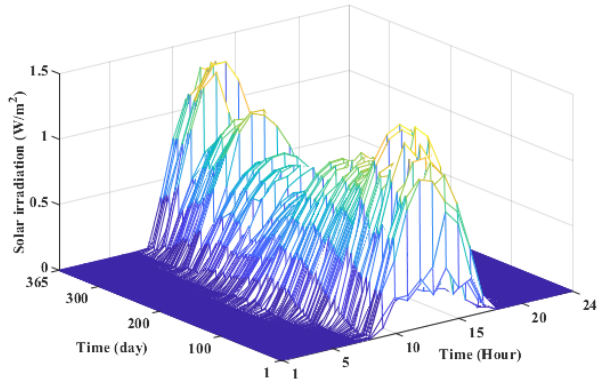
Figure 2. Average hourly solar insolation in a year.
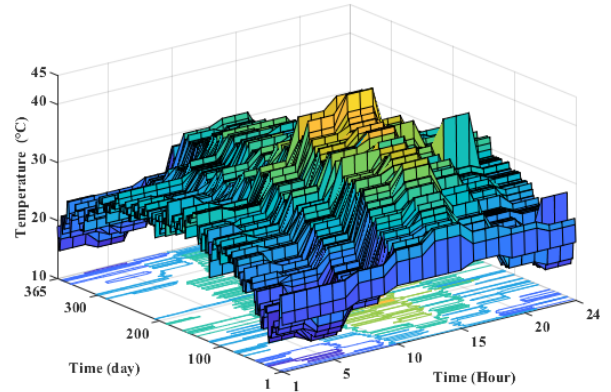
Figure 3. Average hourly ambient temperature in a year.

$$P_{PV} = P_{ratedPV} \times f_{cell} \times \left(\frac{R^2}{R_{STD} \times R_C} \right) \qquad R < R_C$$

$$= P_{ratedPV} \times f_{cell} \times \left(\frac{R}{R_{STD}} \right) \qquad R_C \leq R < R_{STD} \qquad (1)$$

$$= P_{ratedPV} \times f_{cell} \qquad R \geq R_{STD}$$

where P_{PV} denotes the PV output power (kW), R_{STD} denotes the solar irradiance under standard conditions, R_C denotes a particular radiation point, and $P_{ratedPV}$ denotes the PV rated power in kW. The solar irradiation profile for a typical day (1st January 2019) is considered in this study, which is shown as per Figure (4).

The de-rating factor due to temperature is as per Equation (2),

$$f_{cell} = [1 - T_{coeff} \times (T_{module} - T_{ref})] \qquad (2)$$

Where T_{coeff} is temperature coefficient and T_{ref} is reference temperature, which are set at 0.005 and $25^0 C$ respectively. The module temperature T_{module} is calculated as per Equation (3):

$$T_{module} = T_{amb} + \left(\frac{NOC - 20}{800} \right) \times R \qquad (3)$$

Where T_{amb} is the ambient temperature as per Figure (4), and NOC is nominal cell temperature. The parameters of the PV system are as per Table 1.

2.2. Modelling of BESS

In this paper, Valve regulated deep cycle lead acid Batteries are used for the study. These batteries are the most often utilised in solar PV projects, since they are intended for both heavy-duty charging and long life. At the time t, the state of the BESS system is linked to its condition at time $t-1$, the output power of the photovoltaic panel, and the load demand at time t. The parameters of the BESS system is as per Table 1.

1603

Table 1. PV and BESS parameters.

Parameter Name	Specifications
PV Module rating	5kW
R_{STD}	1000 W/m2
R_C	150 W/m2
Nominal operating cell (NOC) temperature of PV cell	$47.6^0 C$
Type of battery module	Valve regulated deep cycle Lead acid
Voltage rating of battery module	12 V
Current rating of battery module	97 Ah
Battery round-trip efficiency (η_{bat})	91 %
SOC_{min}	30 %
SOC_{max}	90 %

The BESS's available capacity at time t may be computed as follows: The capacity of battery during peak hours is expressed as Equation (4)–

$$C_{bat}(t) = C_{bat}(t-1) \times (t-\sigma) \qquad\qquad SOC(t) \leq SOC^{min}$$
$$= C_{bat}(t-1) \times (t-\sigma) - \left[\frac{P_{load}(t))}{\eta_{bat}} - P_{PVac}(t)\right] \qquad SOC(t) > SOC^{min} \qquad (4)$$

The capacity of battery during off-peak hours is expressed as Equation (5)–

$$C_{bat}(t) = C_{bat}(t-1) \times (t-\sigma) \qquad\qquad SOC(t) \geq SOC^{max}$$
$$= C_{bat}(t-1) \times (t-\sigma) + P_{PVac}(t) \times \eta_{bat} \qquad SOC(t) < SOC^{max} \qquad (5)$$

where $C_{bat}(t)$ and $C_{bat}(t-1)$ denote the capacity at t and $t1$, P_{load} denotes the load demand at t, and η_{bat} denotes the round-trip efficiency of the battery. The state of charge (SOC) is evaluated on hourly basis as electricity is supplied to and removed from the battery.

Equation (6) use linear interpolation to estimate the voltage of the BESS while charging and discharging Bhoi et al. [21], where k is the node number, while $N_b(t)$ is the number of batteries connected in series.

$$V_{bat}(t) = [13.5 + 2.4 \times SOC(t)] \times N_b(t) \qquad\qquad, I_{bat} > 0$$
$$V_{bat}(t) = [12.59 - 2.04 \times (1 - SOC(t))] \times N_b(t) \qquad\qquad, I_{bat} < 0 \qquad (6)$$

Charging as per Equation (7),

$$SOC(t) = SOC(t-1) \times (1-\sigma) + \frac{\eta_{chg} \times P_{dc,bat}(t)}{C_{bat}(t) \times V} \qquad (7)$$

Discharging as per Equation (8),

$$SOC(t) = SOC(t-1) \times (1-\sigma) + \frac{\eta_{dischg} \times P_{dc,bat}(t)}{C_{bat}(t) \times V} \tag{8}$$

where $SOC(t)$ and $SOC(t1)$ denote the state of charge (SOC) at hour t and hour $t1$, V denotes the nominal voltage, and $P_{dc,bat}(t)$ denotes the charging/discharging rate of the battery. The charging and discharging schedule and rates have an effect on the BESS's capacity and state of charge. To ensure the effective operation of the BESS, the SOC must remain within permitted limits.

2.3. Modelling of load

Load factor has been determined using test information on hours, days, weeks, and seasons of every bus in the IEEE 69-bus RDS system and has been graphically shown in Figure (5). The actual load demand was estimated using the following Equation (9), taking into account the peak load demand at each bus.
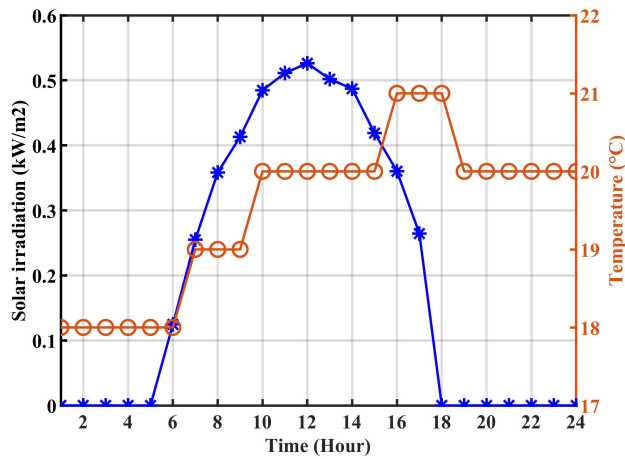
Figure 4. Average hourly solar insolation and temperature in a day.
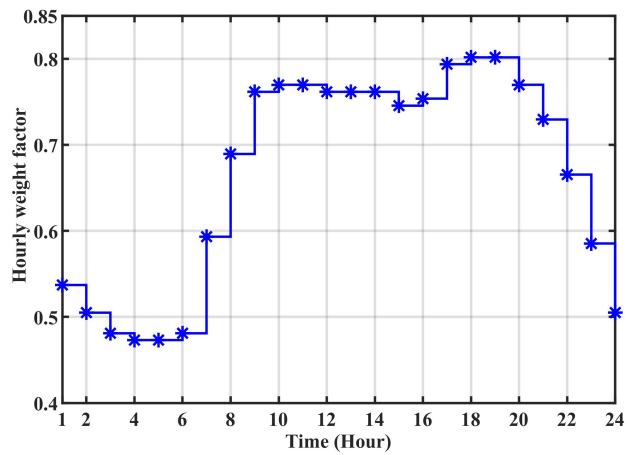
Figure 5. Load weight factor in a day.

At any given time t, the predicted load at bus i can be expressed as per Equation (9):

$$P_{Load,i}(t) = w_h(t) \times P_i \tag{9}$$

where, $w_h(t)$ is the load factor at time t, P_i is the load at i^{th} node of 69-bus RDS system and $P_{Load,i}(t)$ is the actual load at time t for i^{th} node.

3. Problem formulation

The optimum placement and size of PV panel and BESS is defined as per Equation (10), maximizing the benefits from economic gain, reduction in CO_2 emission and reduction in energy loss.

3.1. Objective function

The optimum placement and size of PV & BESS is determined, considering the maximise benefit-cost function, which includes benefits from economic gain per day (energy price arbitrage of a power market, reduction in

transmission access charge, operation, maintenance, replacement & investment cost of PV & BESS) , reduction in CO_2 emission per day and reduction in energy loss per day. The proposed objective function is defined as:

$$Maximise(f_{obj}^1, f_{obj}^2, f_{obj}^3) \qquad (10)$$

3.1.1. Economic gain (f_{obj}^1)

The first objective f_{obj}^1 as per Equation (11), is the benefit-cost function associated with economic gain per day calculated from net present value (NPV) of the project, where C_{ARB} is the benefit from energy price arbitrage, C_{TRANS} is the benefit from reduction in transmission access fees, $C_{O\ \&\ M\ \&\ REP}$ is the PV & BESS operation, maintenance & replacement cost, and $C_{PV\&BESS}$ is the PV & BESS investment cost. Transmission access fees as per Leou et al. [22] (Figure (6)), energy or electricity price arbitrage benefits are estimated on a daily basis in this proposed work. The NPV value of the project is calculated by multiplying its value by the factor $\left(\frac{1+ir}{1+dr}\right)$. The NPV of economic gain is translated to per day economic gain by scaling down using factor of 365. The parameters as per Jannesar et al. [23] are used in this work and summarised in Table 2.

Table 2. Data for optimisation.

Parameter Name	Specifications
Number of planning years	25
Inflation rate (ir)	1.5%
Discount rate (dr)	9%
Battery Round-trip efficiency	91 %
$(C_{Mf,PV} + C_{Mv,PV} + C_{REPCOST,PV})$	Rs. 1.5/$Watt$
$C_{S,PV}$	Rs. 187/$Watt$
$C_{S,B}$	Rs. 32/$Watt$
$C_{WS,B}$	Rs. 7.5/$Watt$
$(C_{Mf,B} + C_{Mv,B})$	Rs. 0.675/$Watt$

$$f_{obj}^1 = max \sum_{j=1}^N \left(\left((C_{ARB} + C_{TRANS}) - \frac{C_{O\ \&\ M\ \&\ REP}}{365} \right) \left(\left(\frac{1+ir}{1+dr}\right)^j \right) \right) - \frac{C_{PV\ \&\ BESS}}{365} \qquad (11)$$

The price of energy is a time-varying and load-dependent variable determined by distribution systems. As a result, DISCO should take advantage of the time-varying nature of power prices while charging and discharging for BESS. The advantage of energy arbitrage is determined as per Equation (12). where $P_{BESS,dischg}^i$ and $P_{BESS,chg}^i$ represents discharge and charge power of battery storage, and ρ_E^i is average energy price in i^{th} h.

$$C_{ARB} = \sum_{i=1}^{24} \left(P_{BESS,dischg}^i - P_{BESS,chg}^i \right) \times \rho_E^i \qquad (12)$$

Transmission operating companies levy transmission Access Fees (as per Figure 6) on distribution companies for the privilege of using energy transmission infrastructure. The energy distribution company (DISCO)

is responsible for paying the transmission access charge based on the hours of the day. The benefit due to reduction in transmission access fee is as per Equation (13). Where ρ_{TRANS}^i is the transmission access fee in i^{th} h.

$$C_{TRANS} = \sum_{i=1}^{24} \left(P_{BESS,dischg}^i - P_{BESS,chg}^i \right) \times \rho_{TRANS}^i \tag{13}$$

$C_{O \& M \& REP}$ denotes the expenses associated with the operation and maintenance of PV and BESS, respectively. The battery is charged and drained once a day in the present paper. where $C_{Mf,B}$ denotes the cost of operation and maintenance of the power converter system and $C_{Mv,B}$ denotes the cost of losses associated with maintaining the power converter system and battery in heated standby mode. Additionally, $C_{Mf,PV}$ and $C_{Mv,PV}$ denote the fixed and variable operating and maintenance costs associated with photovoltaic systems, respectively, while $C_{REPCOST,PV}$ denotes the replacement costs associated with photovoltaic systems, where $(C_{Mf,PV} + C_{Mv,PV} + C_{REPCOST,PV})$ is operation and maintaining cost. PV and BESS costs are comprised of capital and operating expenses. where $C_{S,B}$ and $C_{WS,B}$ denote the expenses associated with the battery's power and energy capacity, respectively. $S_{max,B}$ is the apparent maximum power of BESS, whereas $S_{Wmax,B}$ denotes the optimum energy capacity of BESS. $C_{S,PV}$ denotes the capital cost of photovoltaic solar energy. $P_{max,PV}$ is the maximum power capacity of a photovoltaic system. The expenses of operation, maintenance, and replacement are proportional to the maximum power output, as per Equation (14).

$$C_{O \& M \& REP} = (C_{Mf,B} + C_{Mv,B}) \times S_{max,B} + (C_{Mf,PV} + C_{Mv,PV} + C_{REPCOST,PV}) \times P_{max,PV}$$

$$C_{PV \& BESS} = C_{S,B} \times S_{max,B} + C_{WS,B} \times S_{Wmax,B} + C_{S,PV} \times P_{max,PV} \tag{14}$$

3.1.2. Reduction in CO_2 emission per day (f_{obj}^2)

Conventional power plants are a significant producer of greenhouse gases (CH_4, N_2O, and CO_2). CO_2 is the most potent greenhouse gas, causing the most significant harm to the environment compared to other gases. This emission rate (as per Figure (7)) from generating facilities varies according to load and varies during the day. As a result, the second objective f_{obj}^2 is expressed as the CO_2 emission cost function as Talaei et al. [24] per Equation (15).

$$f_{obj}^2 = max \sum_{i=1}^{24} \left((P_{BESS,dischg}^i - P_{BESS,chg}^i) + P_{PV}^i \right) \times \lambda_{emission}^i \tag{15}$$

where P_{PV} represents the average hourly power of the photovoltaic system, and $\lambda_{emission}^i$ is the average hourly CO_2 emission rate of conventional power plants in i^{th} h.

3.1.3. Reduction in energy loss per day (f_{obj}^3)

PV and BESS's optimal location, size, and operation may result in energy savings since load demand is met by RES and BESS that generate electricity locally rather than through distribution transformers. BESS
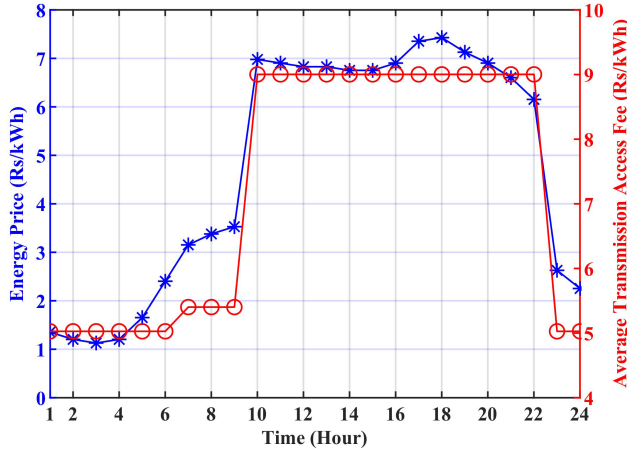
Figure 6. Energy Price & Transmission Access Fee per hour.
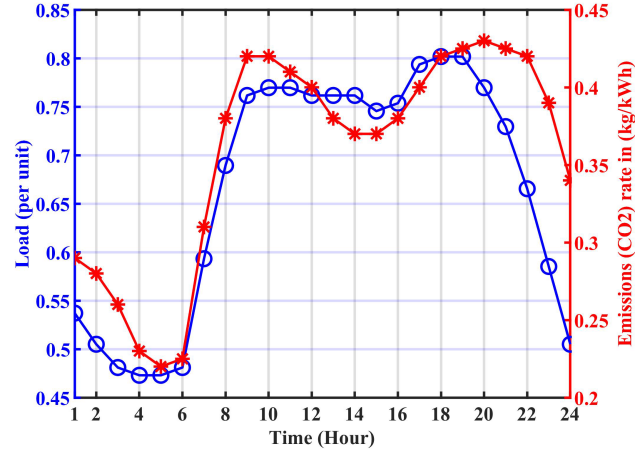
Figure 7. CO_2 Emission rate & load per hour.

charging/discharging is timed to maximise the use of solar energy and to meet peak demand. This third objective f_{obj}^3 is a technological goal, which simulates the decrease of hourly energy losses as described in Equation (16).

$$f_{obj}^3 = max \sum_{i=1}^{24} \left((P_{old,i}^{netloss} - P_{new,i}^{netloss}) \right) \tag{16}$$

where $P_{old,i}^{net_loss}$ and $P_{new,i}^{net_loss}$ represent energy loss before and after optimal placement of PV and BESS, respectively.

3.2. System constraints

Each system component must function within the confines of its respective physical limitations, which are summarised below:

$$P_{sub}(t) = P_{load}(t) + P_{loss}(t) - P_{PV,ac}(t) \mp P_{bat,ac}(t) \tag{17}$$

$$Q_{sub}(t) = Q_{load}(t) + Q_{loss}(t) - Q_{PV,ac}(t) \mp Q_{bat,ac}(t) \tag{18}$$

$$SOC^{min} \leq SOC(t) \leq SOC^{max} \tag{19}$$

$$V_i^{min} \leq V_i(t) \leq V_i^{max} \tag{20}$$

$$P_{PV}^{min} \leq P_{PV}(t) \leq P_{PV}^{max} \tag{21}$$

$$P_{bat}^{min} \leq P_{bat}(t) \leq P_{bat}^{max} \tag{22}$$

$$I_{ij}(t) \leq I_{ij}^{max} \tag{23}$$

where $P_{sub}(t)$, $P_{load}(t)$, $P_{loss}(t)$, $P_{bat,ac}(t)$, $P_{PV,ac}(t)$, $Q_{sub}(t)$, $Q_{load}(t)$, $Q_{loss}(t)$, $Q_{bat,ac}(t)$, $Q_{PV,ac}(t)$, denote power supplied from substation, power delivered to load, power loss, Battery power supplied to/received

from grid , power supplied from PV panel to grid, reactive power supplied from substation, reactive power delivered to load, reactive power loss, Battery reactive power supplied/received from grid and reactive power supplied from PV panel to grid respectively, at time t. SOC^{min} (30%) and SOC^{max} (90%) denote the battery's minimum and maximum charge levels, P_B^{min} and P_B^{max} denote the battery's minimum and maximum DC outputs, P_{PV}^{min} and P_{PV}^{max} denote the PV panel minimum and maximum output power, respectively. $I_{ij}(t)$ is the current across ij^{th} branch at time t and it must be within the maximum allowable limit I_{ij}^{max}. $V_i(t)$ is the voltage at i^{th} node at time t and it must be within the maximum allowable limit of V_i^{min} and V_i^{max} .

3.3. System parameters

The loading of the branch currents in IEEE 69-bus RDS system can be determined using the parameter security margin, which is expressed as percentage loading of rated branch current capacity. The security margin is expressed as Equation (24).

$$min \left(\frac{I_{rated} - I_{actual}}{I_{rated}} \right) \tag{24}$$

4. Multiobjective horse herd optimisation (MOHHOA)

Horse herd algorithm is a meta-heuristic algorithm effective for multiobjective optimisation problems. This algorithm is designed based on the social herding behaviour of horses at different ages. The behaviour evolves and shows distinct patterns as they age. In these age bands, horses' social characteristics like grazing, hierarchy, defence, roaming, imitation, and sociability affect horses' location towards finding optimum space. Different social characteristics cause the unique velocity vector direction, randomness, and mobility across the age groups.

4.1. Mathematical modelling of the MOHHOA

The behaviour pattern of horses is modelled mathematically at different ages. The lifespan of a horse is around 25-30 years. The social behaviour of horses is different during different age groups. The age groups of horses are segregated into four groups, and they are denoted by δ for age ranging about 0-5 years, by γ for age ranging about 5-10 years, by β for age ranging about 10-15 years and by α for age more than 15 years. The movement and location applied to horses depend on the age group of horses, and it is described by Equation (25).

$$X_m^{Iter,AGE} = \vec{V}_m^{Iter,AGE} + X_m^{(Iter-1),AGE}, \qquad AGE = \alpha, \ \beta, \ \gamma, \ \delta \tag{25}$$

In each iteration, a comprehensive matrix response of horses is sorted and based on which the total horse population is segregated into four age groups. The sorted matrix is grouped in first 10% as α horses, next 20% as β horses, following 30% as γ horses, and bottom 40% as δ horses. The velocity vector of horses at different age groups for each iteration of the algorithm can be written as per Equation (26), concerning the different behaviour patterns like grazing (G), hierarchy (H), imitation (I), sociability (S), defence mechanism (D), and roam (R).

$$\vec{V}_m^{Iter,\alpha} = \vec{G}_m^{Iter,\alpha} + \vec{D}_m^{Iter,\beta}$$

$$\vec{V}_m^{Iter,\beta} = \vec{G}_m^{Iter,\beta} + vecH_m^{Iter,\beta} + vecS_m^{Iter,\beta} + \vec{D}_m^{Iter,\beta}$$

$$\vec{V}_m^{Iter,\gamma} = \vec{G}_m^{Iter,\gamma} + vecH_m^{Iter,\gamma} + vecS_m^{Iter,\gamma} + \vec{I}_m^{Iter,\gamma} + \vec{D}_m^{Iter,\gamma} + \vec{R}_m^{Iter,\gamma}$$

$$\vec{V}_m^{Iter,\delta} = \vec{G}_m^{Iter,\delta} + vecI_m^{Iter,\delta} + vecR_m^{Iter,\delta} \tag{26}$$

Individual horses' social intelligence is explored more below.

4.1.1. Grazing (G)

Horses are animals, feed on plants and grasses for which they graze at any age. The algorithm models the motion parameter of ith horse, in accordance with Equation (27).

$$\vec{G}_m^{Iter,AGE} = g_{Iter}(U + p \times L)[X_m^{(Iter-1)}], \qquad AGE = \alpha, \ \beta, \ \gamma \ and \ \delta$$

$$g_m^{Iter,AGE} = g_m^{(Iter-1),AGE} \times \omega_g \tag{27}$$

Here g is the grazing coefficient indicating space around each horse and $\vec{G}_m^{Iter,AGE}$ indicates the tendency of grazing of ith horse. The upper bound of grazing space is U, and the lower bound of grazing space is L, which is set as 1.05 and 0.95, respectively. The grazing coefficient g is set as 1.5 for all age ranges, and p is a random number between 0 and 1. The grazing factor reduces linearity with ω_g per iteration.

4.1.2. Hierarchy (H)

Horses live in herds and are led by a leader. Their tendency to follow the leader is observed during middle ages of β and γ. The coefficient h in the optimisation algorithm is expressed as the propensity of a herd of horses to follow their leader and stronger horses, according to Equation (28).

$$\vec{H}_m^{Iter,AGE} = h_m^{Iter,AGE} \times [X_*^{(Iter-1)} - X_m^{(Iter-1)}], \qquad AGE = \alpha, \ \beta \ and \ \gamma$$

$$h_m^{Iter,AGE} = h_m^{(Iter-1),AGE} \times \omega_h \tag{28}$$

Here $\vec{H}_m^{Iter,AGE}$ shows the relationship of leader horse position on velocity parameter, and $X_*^{(Iter-1)}$ denotes the position of the best horse. The hierarchy factor reduces linearity with ω_h per iteration

4.1.3. Sociability (S)

Horses need social interactions to maintain their security and increase their chances of survival. Predators often hunt them, and it becomes easy to escape in groups. The sociability factor s indicates the tendency of individual horses to move towards the average position of other horses, following Equation (29).

$$\vec{S}_m^{Iter,AGE} = s_m^{Iter,AGE} \left[\frac{1}{N} \sum_{j=1}^{N} X_m^{(Iter-1)} - X_m^{(Iter-1)} \right], \qquad AGE = \beta \ and \ \gamma$$

$$s_m^{Iter,AGE} = s_m^{(Iter-1),AGE} \times \omega_s \tag{29}$$

Here $\vec{S}_m^{Iter,AGE}$ indicates the direction of social motion of ith horse and $s_m^{Iter,AGE}$ indicates the orientation towards herd for the same horse in the middle age groups of β and γ. The sociability factor reduces linearity with ω_s per iteration.

4.1.4. Imitation (I)

Horses mimic one another, and they pick up on both good and negative behaviours through emulating the behaviour of other horses. The imitation factor i indicates the tendency of young horses to mimic other horses, in accordance with Equation (30).

$$\vec{I}_m^{Iter,AGE} = i_m^{Iter,AGE} \left[\frac{1}{pN} \sum_{j=1}^{pN} \widehat{x}_m^{(Iter-1)} - X_m^{(Iter-1)} \right], \qquad AGE = \gamma$$

$$i_m^{Iter,AGE} = i_m^{(Iter-1),AGE} \times \omega_i \tag{30}$$

Here $\vec{I}_m^{Iter,AGE}$ indicates the direction of motion of ith horse toward the $\hat{X}$ location, where $\hat{X}$ is the average of pN number of best horses, and p is set as 10%. The imitation factor reduces linearity with ω_i per iteration.

4.1.5. Defence mechanism (D)

Horses defend themselves by exhibiting situation-based fight-or-flight responses. In this algorithm, the defence factor d is shown as escaping from horses having improper characteristics that are far from optimal, in accordance with Equation (31).

$$\vec{D}_m^{Iter,AGE} = -d_m^{Iter,AGE} \left[\frac{1}{qN} \sum_{j=1}^{qN} \widehat{x}_m^{(Iter-1)} - X_m^{(Iter-1)} \right], \qquad AGE = \alpha, \ \beta \ and \ \gamma$$

$$d_m^{Iter,AGE} = d_m^{(Iter-1),AGE} \times \omega_d \tag{31}$$

Here $\vec{D}_m^{Iter,AGE}$ indicates the direction of escape of ith horse from the $\check{X}$ location, where $\check{X}$ is the average of qN number of horses with worst location, and q is set as 20. Factor d reduces linearity with ω_d per iteration.

4.1.6. Roam (R)

Horses roam around pastures in search of a good location for graze. They tend to discover new places in their neighbourhood randomly. This behaviour is observed predominantly in young horses and diminishes with age. The roaming behaviour is expressed as factor r, following Equation (32).

$$\vec{R}_m^{Iter,AGE} = r_m^{Iter,AGE} \times pX^{Iter-1}, \qquad AGE = \beta \ and \ \gamma$$

$$r_m^{Iter,AGE} = r_m^{(Iter-1),AGE} \times \omega_r \tag{32}$$

Here $\vec{R}_m^{Iter,AGE}$ indicates the velocity of roaming of ith horse to avoid local minima and search space is within the local neighbourhood. The roaming factor reduces linearity with ω_r per iteration.

Figure (8) shows the steps of MOHHOA optimisation applied to the system under study. The best compromised solution is generated from all non-dominated solutions from the archive constituting Pareto-optimal font.
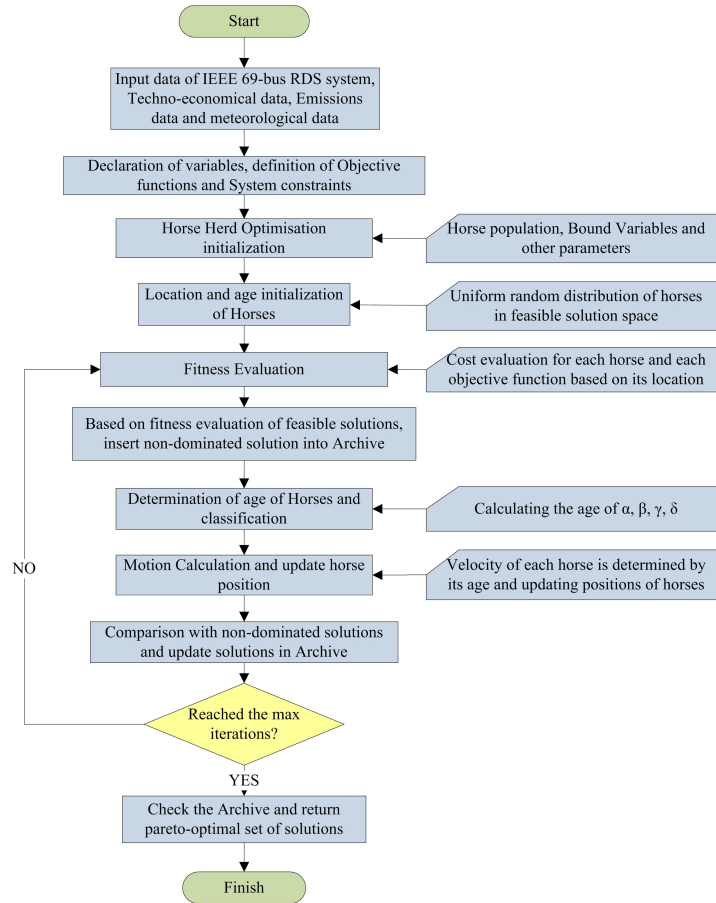
Figure 8. Flowchart of MOHHOA algorithm for optimal PV and BESS allocation.

4.1.7. Best compromised solution using Degree of satisfaction (DS)

This is accomplished by using a fuzzy rule that associates a degree of satisfaction (DS) for every fitness function to any candidate solution in the Pareto optimal set based on the highest and lowest fitness function values obtained in that recursion. The best-compromised solution is determined by the degree of satisfaction DS for each fitness function as per Equation (33).

$$DS_i = \begin{cases} 1 & if f_i \leqslant f_{i,min} \\ \frac{f_{i,max}-f_i}{f_{i,max}-f_{i,min}} & if f_{i,min} < f_i < f_{i,max} \\ 0 & if f_i \geqslant f_{i,max} \end{cases} \tag{33}$$

where i = 1,2,3 due to the fact that this work considers total number objectives ($n_{obj} = 3$). The degree to which the solution vector satisfies all of the goals is then computed as per Equation (34).

$$DS = \frac{1}{n_{obj}} \sum_{i=1}^{n_{obj}} DS_i \tag{34}$$

Following that, the best-compromise solution is chosen by choosing the solution vector with the greatest degree of satisfaction from the collection constraints satisfied of Pareto optimum solutions.

4.2. Application of MOHHOA to solve the problem

Constraints and system data are taken into consideration for optimisation, as are the number of search agents, the total population, the maximum number of iterations, and the design variables (number of RES unit placement buses), which corresponds with the number, position, and capacity of PV and BESS units to be put in the RDS, as well as their restrictions. The optimisation problem considers each cost function in conjunction with its matching objective function. The number of RES units, the number of PV modules, and the number of BESS modules are positive integers. The placement bus, number of PV, and number of BESS of the RES units are generated randomly and normalised to the highest and lowest operating ranges. The flowchart in Figure (8) illustrates the approach for applying the MOHHOA to solve the issue.

4.3. Experiment and discussion

A set of simulation tests was undertaken to evaluate the MOHHOA's performance. Its findings are matched to those of Ali and Khan [25]. A genuine Pareto front is a group of solutions to an optimisation problem that is not dominated by the approximation Pareto front. From the estimated Pareto-front, a collection of equally spaced Pareto optimum solutions (also called nondominated solutions) satisfying the constraints or within the boundary of design space is picked. The suggested method is compared to the previously described techniques using the following two performance criteria.

4.3.1. General distance (GD)

The generational distance as discussed in Van et al. [26], between two points Γ and $\widetilde{\Gamma}$ is a measure of error. It is used to determine the amount to which X and Y are convergent, and it is computed as as per Equation (35):

$$GD = \frac{\sqrt{\sum_{i=1}^{|\widetilde{\Gamma}|} d_i^2}}{\left|\widetilde{\Gamma}\right|} \tag{35}$$

where d_i is evaluated as per Equation (36)

$$d_i = min_{j=1}^{|\Gamma|} |f_i - f_j| \tag{36}$$

where $|\Gamma|$ represents the number of solutions Γ, f_i and f_j represents the objective function value vector of solution i in $\widetilde{\Gamma}$, and j in Γ, respectively. A smaller value of GD guarantees that the $\widetilde{\Gamma}$ approximation error is less.

4.3.2. Diversity metric (DM)

The diversity metric as proposed by Deb et al. [27], quantifies the degree of dispersion in $\widetilde{\Gamma}$. It is defined as per Equation (37)

$$DM = \frac{\left(d_a + d_b + \sum_{i=1}^{|\widetilde{\Gamma}|} \left|\widehat{d_i} - \bar{d}\right|\right)}{\left(d_a + d_b + (\left|\widetilde{\Gamma}\right| - 1)d-\right)} \tag{37}$$

4.3.3. Test instances

There are five benchmark challenges to measure MOHHOA's performance, including SCH, KUR, ZDT1, ZDT3 and ZDT6, which are defined as in Table (3). It comprises the objective functions, variables, and limits for the benchmark problems and the actual Pareto-optimal solutions (D).

Table 3. Benchmark problems.

Benchmark Problem	Minimisation of function (Definition)	Range of variables
SCH	$f_1(x) = x^2, f_2(x) = (x-2)^2$	$x = [-10^3, 10^3]$
KUR	$f_1(x) = \sum_{i=1}^{D} \left(-10e^{-0.2*\sqrt{x_i^2 + x_{i+1}^2}}\right)$ $f_2(x) = \sum_{i=1}^{D} \left(\left|x_i^{0.8}\right| + 5sin(x_i^3)\right)$	$x \in [-5, 5]$ $D = 3$
ZDT1	$f_1(x) = x_1$ $f_2(x) = g(x)[1 - \sqrt{x_1/g(x)}]$ $g(x) = 1 + 9(\sum_{i=2}^{D} x_i)/(D-1)$	$x \in [0, 1]$ $D = 30$
ZDT3	$f_1(x) = x_1$ $f_2(x) = g(x)\begin{bmatrix} [1 - \sqrt{x_1}/g(x)- \\ x_1/g(x)sin10\pi x_1 \end{bmatrix}$ $g(x) = 1 + 9(\sum_{i=2}^{D} x_i)/(D-1)$	$x \in [0, 1]$ $D = 30$
ZDT6	$f_1(x) = 1 - e^{-4x_1}sin^6(6\pi x_1)$ $f_2(x) = g(x)[1 - \sqrt{x_1/g(x)}]$ $g(x) = 1 + 9(\sum_{i=2}^{D} x_i)/(D-1)$	$x \in [0, 1]$ $D = 10$

The tuned values for these MOHHOA parameters are 3, 100, and 250 for the number of objects n, population size s, and a maximum number of iterations n. There have been a total of 50 trial runs. The generational distance and diversity metrics derived from nondominated sorting genetic algorithms -II (NSGA-II), multi-objective particle swarm optimisation (MOPSO), and MOHHOA are compared in Table (4). As shown in Table, MOHHOA consistently gives the best results in terms of GD and DM for each benchmark challenge and also produces more evenly distributed outcomes for all cases.

Table 4. Results of generational distance and diversity metric. (comparison with nondominated sorting genetic algorithm II [NSGA - II] and multiobjective particle swarm optimization [MOPSO]

Benchmark Problem	Parameter	NSGA-II	MOPSO	MOHHOA
SCH	GD (Average)	$8.016e{-}03$	$1.178e{-}01$	$3.457e-04$
	GD (Std dev)	$4.159e{-}03$	$6.209e{-}01$	$2.124e-04$
	DM (Average)	$4.083e{-}01$	1.231	$3.124e-01$
	DM (Std dev)	$3.003e{-}02$	$1.486e{-}01$	$2.314e-02$
KUR	GD (Average)	$5.856e{-}01$	$1.960e{-}01$	$5.836e-03$
	GD (Std dev)	$4.408e{-}01$	$4.486e{-}02$	$1.625e-03$
	DM (Average)	$5.861e{-}01$	1.070	$4.832e-01$
	DM (Std dev)	$9.294e{-}02$	$7.409e{-}02$	$3.684e-02$
ZDT1	GD (Average)	$4.797e{-}02$	$3.156e{-}01$	$2.713e-04$
	GD (Std dev)	$4.985e{-}02$	$1.379e{-}01$	$5.253e-05$
	DM (Average)	$3.653e{-}01$	$9.835e{-}01$	$3.774e-01$
	DM (Std dev)	$4.420e{-}02$	$6.828e{-}02$	$2.652e-02$
ZDT3	GD (Average)	$4.560e{-}02$	$3.308e{-}01$	$3.479e-04$
	GD (Std dev)	$4.538e{-}02$	$2.233e{-}01$	$5.316e-05$
	DM (Average)	$5.823e{-}01$	$8.841e{-}01$	$4.385e-01$
	DM (Std dev)	$4.523e{-}02$	$6.228e{-}02$	$2.357e-02$
ZDT6	GD (Average)	$3.322e{-}01$	$8.938e{-}01$	$5.214e-05$
	GD (Std dev)	$2.507e{-}01$	$8.310e{-}01$	$2.186e-06$
	DM (Average)	1.061	1.193	$3.668e-01$
	DM (Std dev)	$1.484e{-}01$	$1.202e{-}01$	$4.613e-02$

5. Results and analysis

5.1. Case Study

This section implements the suggested PV and BESS planning method in the IEEE 69-bus RDS system. This article makes use of Deep cycle Lead Acid Batteries. The initial state of charge has a maximum of 90% and a minimum of 30%. According to Jannesar et al. [22], the discount rate is 9% when considering the project's 25-year life as discussed.

5.2. Results

A multiobjective framework based on the MOHHOA algorithm is proposed in this study to get the best results for PV & BESS placement and size. Three different configurations of the IEEE 69-bus RDS system are simulated to evaluate the impact of PV and BESS deployment. Table ((5)) shows the simulation scenarios that were chosen for inclusion in this study. For IEEE 69-Bus RDS system cases 1 (base case), 2 (with PV), and 3 (PV & BESS), Figure (9) show the minimum hourly node voltage profile. The voltage across all nodes are within the acceptable range of operational limits and shows improved response in case 3 and case 2 as compared to base case.

Figure (10) shows the comparison of hourly power loss profile for the IEEE 69-Bus RDS system in Case 1 (the basic scenario), 2 (with PV), and 3 (PV & BESS). The hourly power loss reduced significantly in Case 2 and Case 3 as compared to Case 1. Figure (11) show the IEEE 69-Bus RDS system's minimal hourly security margin profile for cases 1 (base case), 2 (with PV), and 3 (PV & BESS). The improvement in security margin for

Table 5. Results of simulated case studies.

Case Study	PV & BESS Bus location	No of PV panel & BESS	Economic gain per day (in Rs)	Reduction in CO_2 emission per day (in kg)	Reduction in energy loss per day (in kWh)	Maximum and minimum voltage in a day (in p.u.)	Minimum security margin in a day (in p.u.)
Case 1	-	-	-	-	-	1.00, 0.9292	0.234
Case 2	62(PV)	406(PV)	1.434×10^6	3.744×10^3	1.464×10^3	1.01, 0.9675	0.405
Case 3	61(PV), 22(BESS)	600(PV), 75(BESS)	2.07×10^6	5.192×10^3	1.423×10^3	1.00, 0.9678	0.407

case 3 (PV & BESS) indicates that the system can accommodate higher load with proper PV and BESS sizing and placement in the radial distribution system. The security margin is lowest during the 18th h because of high loading during that period, and the minimum security margin has improved from 0.234 p.u. to 0.407 p.u. Figure (12) indicates the state-of-charge (SOC) in per unit throughout the day. SOC decreases during peak load period due to discharging of BESS and charging occurs during light load periods. Figure (13) and Figure (14) shows the voltage and current of battery throughout the day. The floating voltage of the battery varies between 15.66 V to 11.35 V during charging and discharging period. The battery current profile indicates the power supplied/consumed from the grid by BESS. The charging and discharging of the BESS can be observed from the state-of-charge of the battery. Figure (15) indicates the multi-objective Pareto-front during optimisation of case 2 and case 3 scenarios, respectively. Best compromised solutions from the Pareto-front are selected based on the degree of satisfaction as per Equation (33).
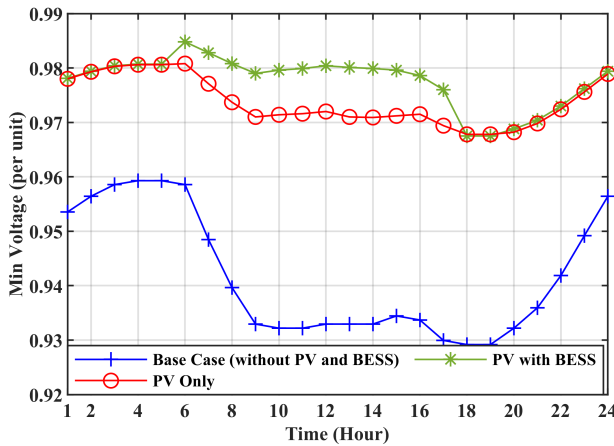
Figure 9. Bus voltage profile in a day
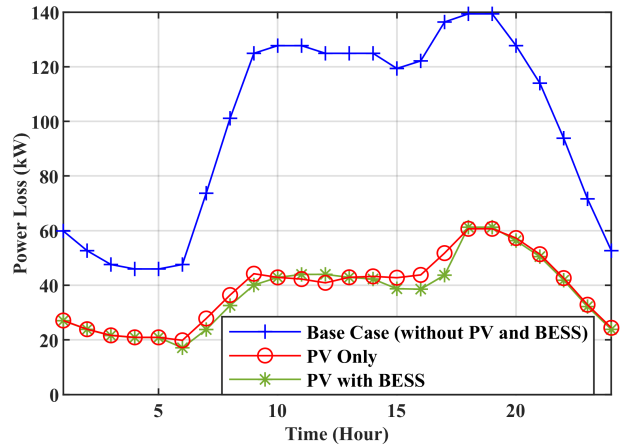
Figure 10. Active power loss in a day.

Table 5 summarises the findings of the instances studied in terms of PV & BESS and sizing, economic gain per day, reduction in CO_2 emission per day, reduction in energy loss per day, maximum and minimum hourly voltage and minimum hourly security margin.

5.3. Discussion on results

Case 1: A low voltage of 0.9292 p.u. is recorded at node 65 during periods of high load. This voltage drop happens during 18-19 h of the day. The daily network energy loss calculated is 2345.9 kWh. The minimum
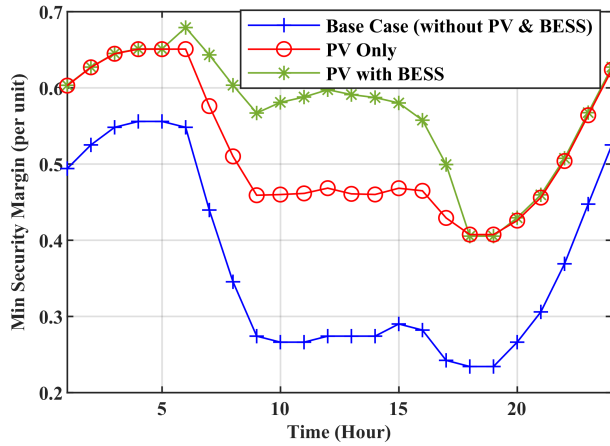
Figure 11. Security margin in a day.
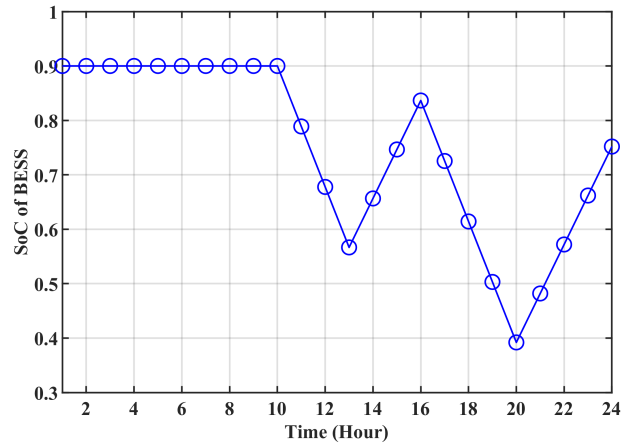
Figure 12. SOC of battery in a day.
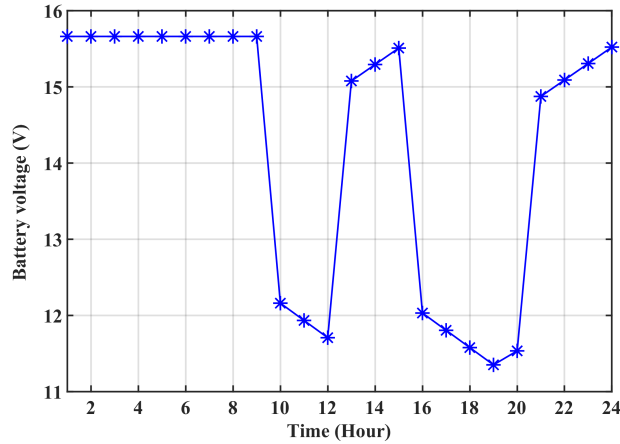
Figure 13. Voltage of battery in a day.
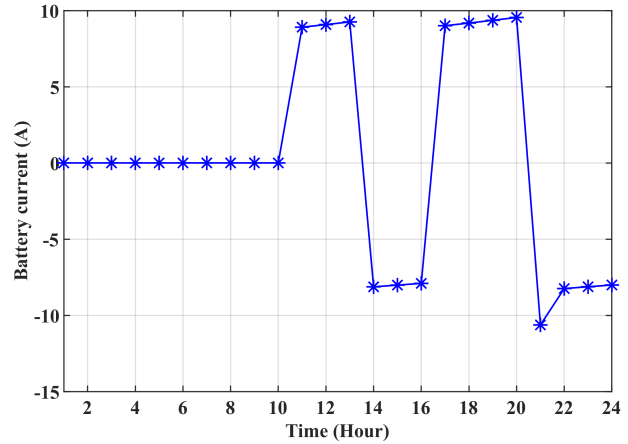
Figure 14. Current of battery in a day.

security margin of 0.234 p.u. is observed during peak hours. Case 2: The PV panel array is placed at node 62 with the capacity of 2030 kW, as indicated in Table 5. Bus 65 had a voltage decrease of 0.9675 p.u. during 18 h of peak load. In this instance, the overvoltage on bus 62 is 1.01 p.u. The reduction in energy loss in the system compared to Case 1 (base case) is 1464.1 kWh. The security margin has improved up to 0.405 p.u. during peak load. The economic savings per day and reduction in CO_2 emissions per day are 1.4345×10^6 Rs and 3.744×10^3 kg, respectively. Case 3: PV panel array is placed at node 61 with the capacity of 3000 kW, and BESS is placed at node 22 with 87.3 kWh capacity. A voltage decrease of magnitude 0.9678 p.u. was recorded during peak load on node 65. There is no overvoltage across any node. The reduction in energy loss in the system compared to Case 1 (base case) is 1423 kWh. The security margin has improved up to 0.407 p.u. during peak load. The economic savings and reduction in CO2 emissions are 2.07×10^6 Rs and 5.192×10^3 kg. Based on these goal functions and with all system parameters kept within their tolerances, the optimum solution with PV allocation is Case 2 and with PV & BESS allocation is Case 3. It was observed that greater economic advantages resulted in decreasing environmental emissions and higher energy losses. Despite the fact that the initial cost of installing RES and BESS is substantial, it was decided that a suitable economic benefit could be
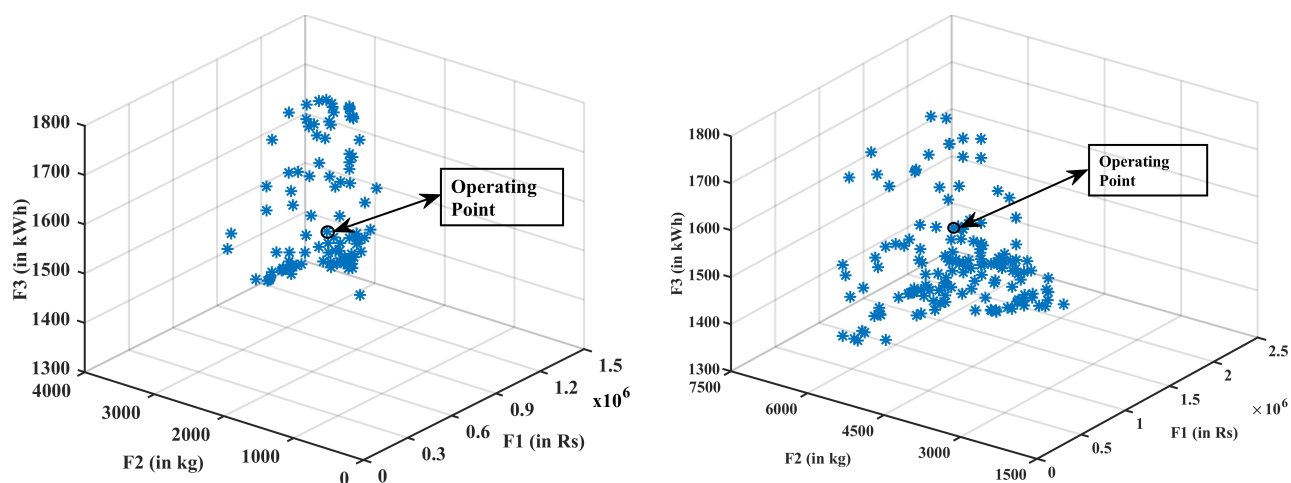
Figure 15. Multiobjective Pareto-front: Economic gain per day, Reduction in CO2 emission per day and reduction in energy loss per day.

reached with careful planning and operation. BESS is charged during low energy prices, transmission access fees, and CO2 emission rates and released at periods of high rates. Additionally, emissions to the environment and energy losses were decreased. Security margins on an hourly basis have improved throughout the system. This research shows inherent promise for solving a multiobjective environmental, technological, and economic issue.

6. Conclusion

In this work, a multiobjective optimisation framework has been designed for concurrent optimal allocation and management of PV and BESS in the IEEE 69-bus RDS. Improved renewable generating capacity of the distribution network is being achieved via the introduction of new objectives as well as additional security constraints. The objective function proposed maximisation of multiple benefits like benefits from economic gain per day, reduction in CO_2 emission per day and reduction in energy loss per day. The performance of the proposed MOHHOA is compared with other multiobjective algorithms. The case studies and simulation results show that the proposed model effectively accommodated PV power generation in IEEE 69-bus RDS without breaching any limits imposed by the system. Similarly, BESS's strategic integration has been optimised, resulting in a considerable increase in the distribution system's techno-economic performance. However, this paper does not attempt to account for the uncertain characteristics of photovoltaics. Future research can address these issues through the use of probabilistic optimisation.

References

[1] Wong L, Ramachandaramurthy V, Taylor P, Ekanayake J, Walker S et al. Review on the optimal placement, sizing and control of an energy storage system in the distribution network; Journal of Energy Storage 2019, 21: 489-504. doi: 10.1016/j.est.2018.12.015

[2] Pawan S, Lata G. An environmental based techno-economic assessment for battery energy storage system allocation in distribution system using new node voltage deviation sensitivity approach. International Journal of Electrical Power & Energy Systems 2021. 128. 106665. doi: 10.1016/j.ijepes.2020.106665

[3] Alam M, Arefifar S. Energy Management in Power Distribution Systems: Review, Classification, Limitations and Challenges; IEEE Access 2019, vol. 7, pp. 92979-93001. doi: 10.1109/ACCESS.2019.2927303

[4] Kalantari N, Hassas M, Pourhossein K. Bibliographic Review and Comparison of Optimal Sizing Methods for Hybrid Renewable Energy Systems; Journal of Energy Management and Technology 2018; 2 (2): 66-79. doi: 10.22109/jemt.2018.102306.1039

[5] Nick M, Cherkaoui R, Paolone M. Optimal Planning of Distributed Energy Storage Systems in Active Distribution Networks Embedding Grid Reconfiguration; IEEE Transactions on Power Systems 2018; 33 (2): 1577-1590 doi: 10.1109/TPWRS.2017.2734942

[6] Saboori H, Hemmati R. Maximizing DISCO profit in active distribution networks by optimal planning of energy storage systems and distributed generators; Renewable and Sustainable Energy Reviews 2017; 71: 365-372 doi: 10.1016/j.rser.2016.12.066

[7] Talent O, Du H, Optimal sizing and energy scheduling of photovoltaic-battery systems under different tariff structures; Renewable Energy 2018; 129: 513-526: doi: 10.1016/j.renene.2018.06.016

[8] Salehi J, Esmaeilpour S, Samadi F, Safari A. Risk Based Battery Energy Storage and Wind Turbine Allocation in Distribution Networks Using Fuzzy Modeling; Journal of Energy Management and Technology 2018; 2 (2): 53-65. doi: 10.22109/jemt.2018.104786.1046

[9] Mahdavi S, Hemmati R, Mehdi A. Two-level planning for coordination of energy storage systems and wind-solar-diesel units in active distribution networks; Energy Elsevier 2018; 151: 954-965. doi: 10.1016/j.energy.2018.03.123

[10] Li Y, Feng B, Li G, Qi J, Zhao D et al. Optimal distributed generation planning in active distribution networks considering integration of energy storage; Applied Energy 2018; 210: 1073-1081 doi: 10.1016/j.apenergy.2017.08.008

[11] Mahmood D, Javaid N, Ahmed G, Khan S, Monteiro V. A review on optimization strategies integrating renewable energy sources focusing uncertainty factor – Paving path to eco-friendly smart cities; Sustainable Computing: Informatics and Systems 2021; 30: 100559 doi: 10.1016/j.suscom.2021.100559

[12] Li C, Yu X, Huang T, Chen G, He X. A Generalized Hopfield Network for Non-smooth Constrained Convex Optimization: Lie Derivative Approach; IEEE Transactions on Neural Networks and Learning Systems 2016; 27 (2): 308-321. doi: 10.1109/TNNLS.2015.2496658

[13] Li C, Yu X, Huang T, He X. Distributed Optimal Consensus Over Resource Allocation Network and Its Application to Dynamical Economic Dispatch; IEEE Transactions on Neural Networks and Learning Systems 2018; 29 (6): 2407-2418. doi: 10.1109/TNNLS.2017.2691760

[14] Naeimi F, Azizyan G, Rashki M. Horse herd optimization algorithm: A nature-inspired algorithm for high-dimensional optimization problems; Knowledge-Based Systems 2021; 213: 106711. doi: 10.1016/j.knosys.2020.106711

[15] Mikaeel A, Mohammed L, Shah D, Ryuto S, Atsushi Y et al. Optimal Multi-Configuration and Allocation of SVR, Capacitor, Centralized Wind Farm, and Energy Storage System: A Multi-Objective Approach in a Real Distribution Network; IET Renewable Power Generation 2019; 13 (5): 762-773 doi: 13.10.1049/iet-rpg.2018.5057

[16] Das CK, Bass O, Kothapalli G, Mahmoud T, Habibi D. Overview of energy storage systems in distribution networks: Placement, sizing, operation, and power quality; Renewable and Sustainable Energy Reviews 2018; 91:1205-1230 doi: 10.1016/j.rser.2018.03.068

[17] Duchaud J, Darras C, Notton G, Cyril V. Multi-Objective Particle Swarm Optimal Sizing of a Renewable Hybrid Power Plant with Storage; Renewable Energy 2018; 131:1156-1167 doi: 10.1016/j.renene.2018.08.058

[18] Bakhtiari H, Naghizadeh R. Multi-criteria optimal sizing of hybrid renewable energy systems including wind, photovoltaic, battery, and hydrogen storage with ϵ-constraint method; IET Renewable Power Generation 2018; 12: 883-892. doi: 10.1049/iet-rpg.2017.0706

[19] Sawle Y, Gupta S, Bohre A. Socio-techno-economic design of hybrid renewable energy system using optimization techniques; Renewable Energy 2018; 119: 459-472 doi: 10.1016/j.renene.2017.11.058

[20] Bhoi SK, Nayak MR, Kasturi K. Energy scheduling of grid-tied photovoltaic-wind-diesel-battery hybrid system for load management under real-time pricing mechanism using game theory; Turkish Journal of Computer and Mathematics Education 2021; 12 (6): 5033-5044.

[21] Bhoi SK, Nayak MR. Optimal scheduling of battery storage with grid tied PV systems for trade-off between consumer energy cost and storage health; Microprocessors and Microsystems 2020; 79: 103274. doi:10.1016/j.micpro.2020.103274

[22] Leou RC. An economic analysis model for the energy storage system applied to a distribution substation, International Journal of Electrical Power & Energy Systems 2012; 34 (132-137). doi:10.1016/j.ijepes.2011.09.016

[23] Jannesar M, Sedighi A, Savaghebi M, Guerrero J. Optimal placement, sizing, and daily charge/discharge of battery energy storage in low voltage distribution network with high photovoltaic penetration; Applied Energy 2018; 226: 957-966 doi: 10.1016/j.apenergy.2018.06.036

[24] Talaei A, Begg K, Jamasb T. The large scale roll-out of electric vehicles: the effect on the electricity sector and CO2 emissions, EPRG Working Paper 2012 doi:10.17863/CAM.1017

[25] Ali H, Khan FA. Attributed multi-objective comprehensive learning particle swarm optimization for optimal security of networks. Applied Soft Computing. 2013; 13 (9):3903-3921. doi:10.1016/j.asoc.2013.04.015

[26] Van Veldhuizen DA, Lamont GB. Evolutionary computation and convergence to a pareto front. In Late breaking papers at the genetic programming 1998 conference 1998 Jul 22 (pp. 221-228).

[27] Deb K, Pratap A, Agarwal S, Meyarivan TA. A fast and elitist multi-objective genetic algorithm: NSGA-II. IEEE Transactions on Evolutionary Computation 2002;6 (2):182-197. doi:10.1109/4235.996017